Al$_2$O$_3$ Collection and Sizing from Solid Rocket Motor Plumes

Jay K. Sambamurthi*
NASA Marshall Space Flight Center, Huntsville, Alabama 35812

A unique dart system has been designed and built to collect aluminum oxide particles from the plumes of large-scale solid rocket motors, such as the Space Shuttle redesigned solid rocket motor (RSRM). The capability of this system to collect clean samples from both the vertically fired modified NASA (MNASA) (18.3% scaled version of the RSRM) motors and the horizontally fired RSRM motor has been demonstrated. The particle mass-averaged diameters d_{43} measured from the samples for the different motors, ranged from 8 to 11 μm and were independent of the dart collection surface and the elapsed time during motor burn. The measured d_{43} results agreed well with those calculated using the industry standard Hermsen's correlation within the standard deviation of the correlation. For each of the samples analyzed from both MNASA and RSRM motors, the distribution of the cumulative mass fraction of the plume oxide particles as a function of the particle diameter was best described by a monomodal log-normal distribution with a standard deviation between 0.13–0.17. This distribution agreed well with the theoretical prediction by Salita using the one-dimensional three phase code for the RSRM motor at the nozzle exit plane; this seems to confirm that droplet collision–coalescence removes most of the smoke mass from the plume flowfield.

Introduction

THERMAL radiation from the plume of any solid rocket motor containing aluminum as one of the propellant ingredients, is mainly from the 0.1- to 20-μm hot aluminum oxide (Al$_2$O$_3$) particles in the plume. The plume radiation to the base components of a flight vehicle is primarily determined by the plume flowfield properties, the size distribution of the plume particles, and their optical properties. The optimum design of a vehicle base thermal protection system (TPS) is dependent on the ability to predict accurately this intense thermal radiation using validated theoretical models.

Currently, the design thermal radiation to the base region of the shuttle components from the redesigned solid rocket motor (RSRM) plumes is predicted using a simple empirical model[1] based on flight measured data. However, a more advanced reverse Monte Carlo method[2] has been developed recently for the advanced solid rocket motor (ASRM) program. This model is currently being validated using measured radiation data from flight motors as well as static firing of the full-scale motors at the Thiokol Space Operations Facility in Utah and the 18.3% scaled modified NASA (MNASA) motors at NASA/Marshall Space Flight Center (MSFC). Such validations enable one to gain confidence in the Monte Carlo model. Application of this model to the RSRM design thermal radiation environments is expected to improve the current designs and to reduce the TPS requirements in the base region of the shuttle.

A major unknown in the input to the theoretical Monte Carlo radiation model is the size distribution of Al$_2$O$_3$ particles in the plume. Previously, no measured plume particle size distribution existed for a full-scale RSRM, so that the model used a theoretical distribution[3] that consisted of five equal mass fractions based on a normal distribution about a mass-averaged

diameter d_{43}. However, radiation predictions made using this distribution were conservative when compared with measured data. Consequently, it was decided to measure the particle size distribution in the plume to improve the radiation predictions. A dart collection method was chosen that had already proven successful in MNASA motor firings.

To anticipate and interpret the results of these measurements, existing plume data were reviewed. Salita[4] has summarized the recent attempts to measure Al$_2$O$_3$ particle size in solid rocket motor chambers, nozzles, and plumes. Six of the 19 studies he summarized related to collection of plume particles from solid rocket motors, varying in size from very small micromotors to large Titan motors. The data fell into two groups: 1) only large particles (>2 μm) were recovered[5,6] or 2) only submicron particles (<2 μm) were recovered.[7-9] The inconsistency of these results is obviously because of the biases of the different collection techniques.

Large median diameters in plumes have been reported by numerous authors. Hermsen[5] correlated a wide range of previously reported size data, but did not include any full-scale motors of the RSRM size. Kohlbeck et al.[6] have collected plume particles from several large motors and observed Al$_2$O$_3$ particles in the 0.5 to 8 μm range that agreed with Hermsen's correlation. Salita[10] used a corrected version of the one-dimensional three phase (OD3P) code and an improved model of droplet collision/coalescence to predict that the bimodal distribution of droplet size measured in quench bombs simulating RSRM chamber, becomes monomodal in the nozzle because most of the mass of smoke droplets collides and coalesces with the larger droplets. The results also indicated that the predicted size distribution entering the plume contained only 2% mass of smoke (although roughly 50% number fraction of smoke), whereas the remaining droplet mass had a standard deviation of 0.13 and a d_{43} in agreement with Hermsen's correlation.

Meanwhile, only smoke has been reported by numerous authors. Dill et al.[7] have sampled plume particles from a small inertial upper stage (IUS) motor. Here, the samples were collected by a probe placed 8 ft downstream of the nozzle exit plane. There were no differences in the samples obtained at the edge or centerline of the plume. However, the absence of the large particles in the samples seemed to indicate that only the smoke particles were collected by the probes. To study the impact of Titan launches on the environment, Strand et al.[8] sampled the plume particle filled atmosphere immediately after

*Aerospace Engineer, M/S ED33. Senior Member AIAA.

Titan launches. However, these particle collection systems were not located in the plume during the actual firing of the motor. They collected samples 7–23 min after the passage of the vehicle by flying through the plume trail in a helicopter and a U-2 plane. The large particles might have settled long before the actual collection of the particles. Laredo et al.[11] investigated the oxide particle size inside and in the plume of micromotors (0.5-cm throat diameter) with RSRM propellant using both optical- and probe-impingement techniques. Salita's analysis of Laredo's results indicated that the measured d_{43} was twice that of Hermsen's prediction, even though 53% of the plume particle mass was smaller than 2 μm, in contrast to the prediction of 1–2% by Salita.[10] This contradiction in result could be because of the presence of a few exceptionally large particles in the plume. After further studies with these micromotors, Gomes et al.[12] determined the presence of unusually large particles in the plume because of periodic accumulation and shedding of large agglomerates from the very small diameter nozzle throats.

All of the plume particle collection techniques described previously have been successful in collecting either only submicron particles[7–9] or larger particles,[5,6] but not both sizes with the same technique. Each experimental technique seems to be biased either to the smoke mode or coarse mode. However, both modes exist simultaneously in the plume, and the only way to quantify their coexistence may be through analytical techniques like those of OD3P. It will be shown that the results of the current test program are in agreement with the predictions of OD3P.

This article describes a successful effort to collect plume particle samples from the static firing of large solid rocket motors, and to measure the d_{43} and the size distribution of the Al_2O_3 particles from these samples. The motors investigated included the RSRM designated as flight support motor no. 4 (FSM-4) testfired at the T-24 test stand at the Thiokol Space Operations Facility in Utah, as well as three 18.3% scaled MNASA motors (MNASA 8–10) tested at NASA/MSFC. Prior attempts to collect plume particles from full-scale motor firings have been unsuccessful because of the extremely hostile thermal and acoustic environment in the vicinity of the motor nozzle.

Particle Collection Method

A plumbing schematic of the plume particle collection system is presented in Fig. 1. The principle behind this particle collection technique is to pneumatically launch darts through the plume during the motor firing and collect the plume particle samples on sticky copper tapes mounted at different locations on the dart.

The pneumatic system used in collecting plume particles from full-scale RSRM motor consisted of a launcher with a bank of four accumulators (A-017–A-047) and an electronic control box. Each accumulator was connected through a check valve (CV-013–CV-043) to a common high-pressure nitrogen source and a solenoid valve as shown in Fig. 1. Also, each accumulator was connected to a launch tube through a high
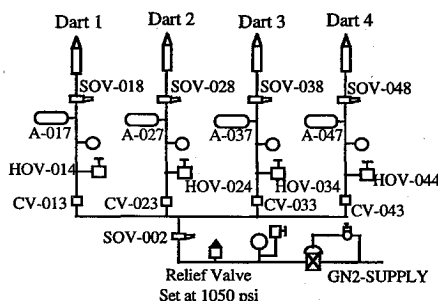
flow rate valve activated by a solenoid. These four valves and solenoids are indicated as SOV-018, 028, 038, and 048 in Fig. 1. To prepare for launching, individual darts were inserted over each launch tube, the solenoid valves were closed by the control box to ensure no leakage of high-pressure gas into the launch tube, and the accumulators were loaded with high-pressure nitrogen to 800 psi. The darts were launched individually by opening the high flow rate valves using the solenoids triggered by a time sequencer in the control box. The control box time sequencer was initiated by the motor firing sequencer at ignition. Each accumulator was also provided with a safety hand valve (HOV 014–044) for bleeding the accumulator in the event of a misfire or delay in the static test.

The first pneumatic system was built for MNASA 8 test and used only one accumulator with one launch tube. After its success, four more accumulators, launch tubes, and associated plumbing were added to the pneumatic system for launching five darts in MNASA 9 and 10 tests. However, because of transportation limitation of the five-dart launch system to Thiokol space operations facility at Utah and reduced reliability on one of the five accumulators in holding the high-pressure nitrogen, one of the accumulators and launch tubes was disconnected from the five-dart launch system for the full-scale RSRM test. The general description of the plumbing for the pneumatic system presented in the previous paragraph applies to all of the tests described in this investigation.

MNASA Method

A simple 42-in. dart, weighing about 13 lb (Fig. 2a), was utilized in three MNASA tests. The Al_2O_3 plume particles were collected by sticky copper tapes affixed at different locations on the shaft and fins of the dart, as well as on stainless-steel wires of diameters varying from 1/4 to 1/32 in., welded around the dart. Agreement in the size distribution of the particles collected at these different locations would improve confidence in the results.

The MNASA motors were tested vertically upward with the exit plane of the nozzle located about 30 ft above the ground. The general characteristics of the motors, MNASA 8–10, are given in Table 1. The launcher was located 55 ft from the motor centerline. The darts were launched at 80 deg measured from the horizontal and had an approximate launch velocity of 125 ft/s. It was estimated to enter the plume at about 150 ft from the nozzle exit plane and exit at about 620 ft, with a residence time of about 5 s in the plume. The darts landed nose first and buried up to 1.5 ft into the ground. However, the plume samples collected by the copper tapes on the steel
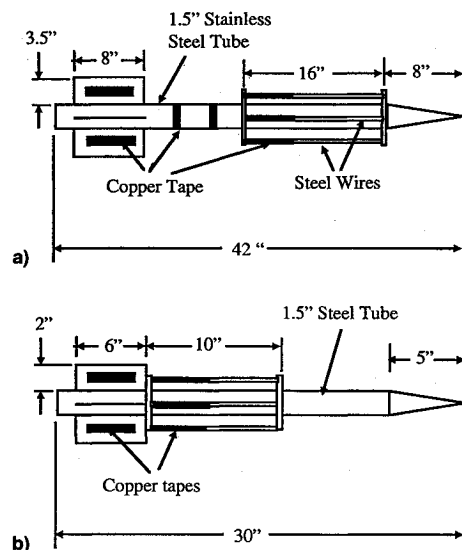

Fig. 2 a) Dart launched through the plume in MNASA tests and b) control dart launched through the plume in full-scale RSRM test.

Fig. 1 High-pressure plumbing schematic diagram for the dart system.

Table 1 General characteristics of the MNASA motor tests where plume particles were sampled

Motor feature	MNASA 8	MNASA 9	MNASA 10
Nozzle	Contour	Conical	Conical
Throat D, in.	9.986	9.958	9.958
Expansion ratio	7.583	5.5587	5.5587
Propellant	ASRM	RSRM	RSRM
% aluminum	19	16	16
Chamber pressure, psi	624	717	650

Fig. 3 Tethered dart employed in the FSM-4 test.

wires remained mostly uncontaminated during ground impact of the dart.

In the MNASA 8 test, one dart was launched 1 s after motor ignition; in the MNASA 9 test, five darts were launched at 1, 3, 5, 7, and 15 s after ignition; and in the MNASA 10 test, five darts were launched at 1, 3, 5, 7, and 9 s after ignition. All of the darts were successful in collecting particles from the plume. Darts 3 and 4 of the MNASA 10 test did not land nose forward. Hence, the samples were severely contaminated and were not included in the size-distribution analysis.

RSRM Method

The full-scale RSRM static test motor was fired horizontally. The motor centerline is about 10 ft above ground level and the motor is fired into a hill about 800 ft aft of the nozzle exit plane.

For the FSM-4 test, the dart system was located 285 ft aft of the nozzle exit plane and about 200 ft from the motor centerline. The plume diameter at 285 ft aft of the nozzle is estimated to be about 90 ft. The aim point of the darts was dictated by the need for the darts to survive the high dynamic pressure of the plume. The dynamic pressure is considerably reduced near the outer boundary of the plume, which improves the survivability of the dart. Consequently, the launch angles of the darts were such that they were aimed about 10–20 ft below the upper boundary of the plume and perpendicular to the plume axis. Moreover, the higher launch angle of the dart increased the range of the dart's trajectory and protected the dart from the hostile exhaust environment after its traverse through the plume. The plume height also minimized the contamination by dust and dirt entrained from the ground by the motor plume.

Two different types of darts were launched in the FSM-4 test. One of them was a control dart (Fig. 2b) weighing about 6 lb, and was basically a scaled version of the dart (Fig. 2a) employed in the MNASA program. It was employed here because of its success in collecting plume samples from the MNASA motor. The dart's weight was scaled down to 6 lb from the MNASA version to increase its range to the desired 400 ft. However, because of the orientation of the RSRM motor during the static test, a large recirculating cloud of dust and dirt is created as the plume impacts the hill aft of the nozzle. The copper tapes affixed to the control dart would be exposed to this dust and dirt after its traverse through the plume. This was expected to result in difficulty of discriminating the plume particles in the samples collected by the tapes. Consequently, a new dart design was needed to keep the copper tapes collecting the plume particle sample contaminant free until the darts could be retrieved.

The new dart designed to minimize the contamination of the copper tapes collecting plume samples from the full-scale RSRM test is shown in Fig. 3. The plume particle samples were collected on 10-in. copper tapes affixed to a stainless-steel tube 1.5 in. in diameter. A cylindrical sleeve, activated by a plate–pulley mechanism and attached to a 240-ft tether, slid over the sampling area to protect the sample after it was collected in the plume. The sleeve was also designed with a positive latch mechanism to prevent opening of the sleeve upon ground impact. Both the 1.5-in. sample tube and the cylindrical sleeve were inserted over an aluminum shaft 48 in.
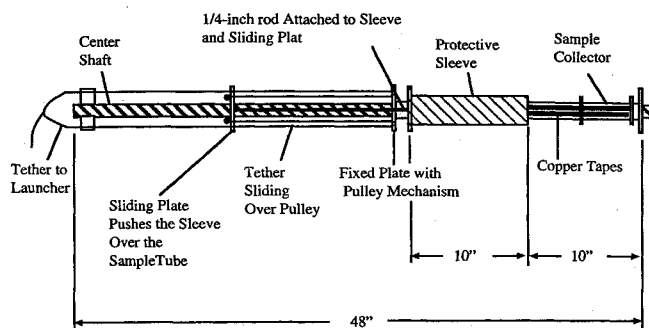
in length. The tether was a 1/16-in.-diam steel wire wound around an inverted canister. The tail end of the tether was attached to a hook on the launcher and the head end to the plate–pulley mechanism on the dart. When the end of the tether was reached during the flight of the dart, the tether pulled the cylindrical sleeve over the sample area and disengaged the sample-collecting tube with the sleeve from the center aluminum shaft. The sample with its protective shield followed a ballistic path and safely landed on the other side of the plume. The aluminum shaft stayed attached to the tether and was destroyed by the plume. The length of the tether was selected such that the sleeve was engaged over the sample area when the dart was just about to leave the plume.

Individual protective housings were also built over the darts on the launcher to protect the darts from contamination between motor ignition and dart launch. In addition, sand bags were placed on all ground electrical connections to prevent disconnection during ground vibration.

In the FSM-4 test, the tethered darts were launched at 12.3, 67.0, and 93.5 s and the control dart was launched at 68.3 s after motor ignition. All four darts were launched during three separate nozzle pitch-up events, which elevated the plume by about 25 ft at 300 ft aft of the nozzle exit plane. This further ensured the ability of the darts to collect relatively clean samples from the plume. The residence time of the darts in the plume was estimated to be about 0.5 s. Both dart designs weighed about 6 lb.

The two tethered darts launched at 12.3 and 93.5 s, and the control dart launched at 68.3 s, functioned nominally. The range of the darts in the absence of the plume was measured to be about 400 ft and was increased by about 50 ft because of the influence of the plume. The cylindrical sleeves on the tethered darts were completely secured. The cylindrical sleeve mechanism was not activated on the third tethered dart because of breaking of the tether during the launch of the dart.

Results

Scanning electron microscope (SEM) analysis of the copper tapes from the different darts revealed a large collection of mostly spherical plume particles. Typical SEM micrographs of the samples from the MNASA tests and the FSM-4 test are shown in Figs. 4a and 4b, respectively. The majority of the particles had a smooth surface and appeared dark brown under an optical microscope. The diameter of the particles varied from submicron to 16 μm in the MNASA samples, and from 1–40 μm in the FSM-4 samples. The size distribution for a given sample was determined by measuring individual particles on enlarged SEM photographs using a scanner and a Macintosh personal computer.

The measured mass-averaged diameter d_{43} for a collected sample was determined from

$$d_{43} = \sum d_i^4 \bigg/ \sum d_i^3 \qquad (1)$$

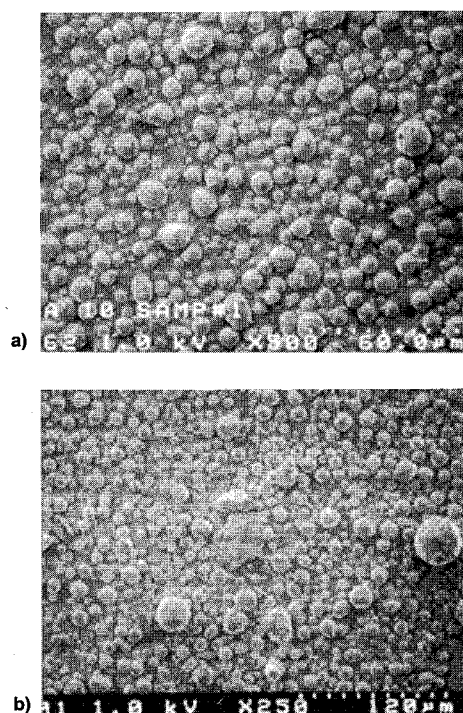where the summation was carried over all of the particles in

Fig. 4 Typical plume particles sample from a) MNASA test and b) FSM-4 test (tethered dart).
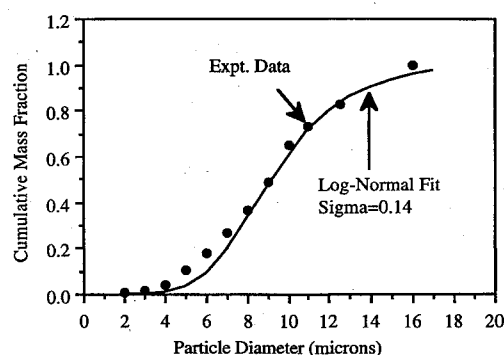

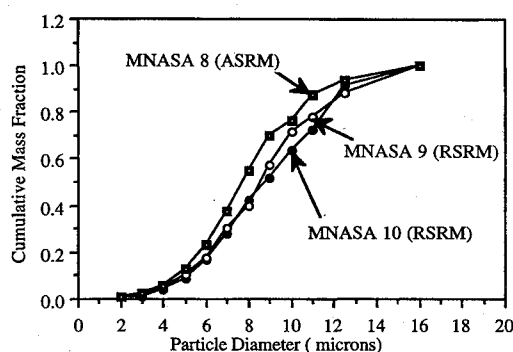Fig. 5 Cumulative mass fraction for plume particle sample collected by dart 1 of MNASA 9 test.

Fig. 6 Comparison of size distribution of plume particles collected by the shaft of dart 1 in the three MNASA tests.
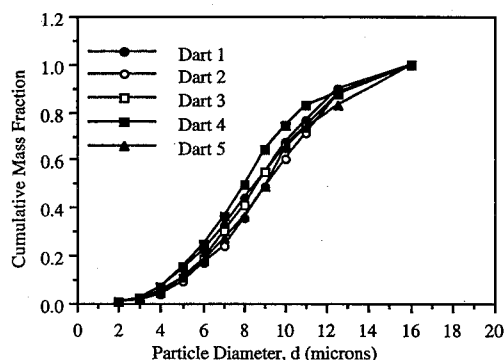

Fig. 7 Comparison of size distribution of plume particles collected by darts 1–5 in MNASA 9 test.

the sample. All measured particle sizes in this report were at room temperature.

The dart results were compared to the industry standard, the Hermsen correlation for calculating d_{43} for solid rocket motor plume particles at the nozzle exit plane, given by

$$d_{43}\ (\mu m) = 3.6304 D_t^{0.293}[1.0 - \exp(-0.0008163\xi_c P_c \tau)] \quad (2)$$

where D_t is the throat diameter in inches (see Table 1 for the MNASA motors and 53.86 in. for the RSRM motor), ξ_c is the Al_2O_3 concentration inside the chamber in g-mole/100 g (0.262 for the RSRM propellant and 0.3 for the ASRM propellant); P_c is the chamber pressure in psia (see Table 1 for the MNASA motors, about 880 psi at 12.3 s and about 630 psi at 68.3 s for the FSM-4 motor); and τ is the average residence time in the chamber (estimated to be about 120 ms for the MNASA motor and 350 ms for the RSRM motor).

MNASA Motors

In all of the MNASA samples examined, the number of particles in each sample exceeded 1000. The mass distribution of these particles is shown in Figs. 5–8. In a given sample, all particles under 2 μm were grouped into one size with a mean size of 1 μm. In all MNASA samples examined, nearly 80% of the particles measured were under 4 μm, but the mass-median diameter was always between 7.5–9.0 μm.

The measured d_{43} from each of the MNASA samples analyzed is compared in Table 2 to the value calculated from Hermsen's correlation. The measured d_{43} is always 10–30% higher than the calculated value, but within the standard deviation of the correlation, $\sigma = 0.298$ (corresponding to a deviation in d_{43} of about ±35%).

Figure 5 shows the cumulative mass fraction plotted against the plume particle size for one of the samples analyzed. Also shown in the figure is the best fit of the data, a log-normal distribution with a standard deviation of 0.14. The size distribution of each MNASA sample analyzed was best curve-fitted by a log-normal monomodal distribution with the standard deviation varying from 0.13 to 0.17.

In addition to the previous general trends, the following features were observed:

1) Figure 6 shows a comparison of the size distributions of the particles collected on the shaft of the dart launched 1 s after motor ignition in MNASA 8–10 tests. The size distribution is not significantly different among the different motors. The fact that motors 9 and 10 were identical to motor 8, except for the propellant formulation and expansion ratio, suggests that plume particle size is relatively independent of percentage aluminum and the nozzle expansion ratio. This is consistent with Hermsen's correlation, which says that plume particle size depends principally on throat diameter.

2) Figure 7 shows a comparison of the size distribution of the particles collected by the 1/4-in.-diam wire on darts 1–5 from MNASA 9 test. The distribution is not significantly different among samples from different darts, indicating the absence of any variation in plume particle size distribution with elapsed time during motor burn.

3) Figure 8 shows a comparison of the size distribution of the particles collected on the shaft and the 1/4- and 1/16-in.-diam wires from the dart in MNASA 9 test. Though the finer wires, as expected, indicate slightly higher mass fractions of smaller particles, the distributions do not appear to be signif-

Table 2 Measured and calculated mass-averaged diameter for the samples of MNASA plume particles analyzed

Sample/test	Measured	Hermsen	% difference
D-1/S/MNASA 8	7.98	7.15	11.61
D-1/S/MNASA 9	8.57	7.17	19.53
D-1/14"T/MNASA 9	8.45	7.17	17.85
D-1/1/16"T/MNASA 9	8.19	7.17	14.23
D-2/1/4"T/MNASA 9	9.17	7.17	27.90
D-3/1/4"T/MNASA 9	8.69	7.17	21.20
D-4/1/4"T/MNASA 9	8.22	7.17	14.64
D-5/1/4"T/MNASA 9	9.21	7.17	28.45
D-1/S/MNASA 10	8.86	7.18	23.40
D-1/1/4"T/MNASA 10	8.40	7.18	16.70
D-2/1/4"T/MNASA 10	8.89	7.18	23.82
D-3/1/4"T/MNASA 10	8.40	7.18	16.70

Note: S and T represent shaft and tube, respectively, and D stands for dart.
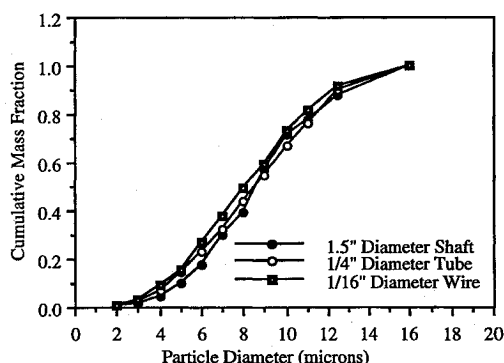
Fig. 8 Comparison of size distribution of plume particles collected on different surfaces of dart 1 in MNASA 9 test.
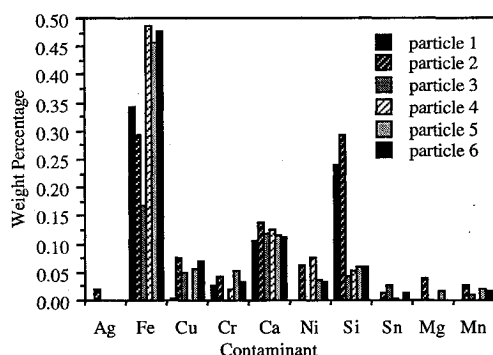
Fig. 9 Electron microprobe analysis of a few MNASA 8 plume particles using wavelength dispersive spectrum.

icantly different. Nearly 80% of the particles collected by the shaft were under 4 μm, indicating that the bias in the size distribution of the particles collected by the shaft of the darts is negligible.

To assure that the diameter of the spherical particles measured from the MNASA tests was that of the plume particles primarily containing aluminum oxide, the composition of the particles was determined from the wavelength-dispersive spectrum of individual particles. This was done using an electron microprobe on randomly selected particles and is illustrated in Fig. 9. Moreover, the optical properties of the Al_2O_3 plume particles (both solid and molten) are functions of the contaminants in them.[13] The contaminants detected included Ag, Fe, Cu, Cr, Ca, Ni, Si, Sn, Mg, and Mn, and their individual levels were under 1% by weight. The source of individual contaminant is unknown. However, the original aluminum particles in the propellant formulation have a small percentage of iron contamination. The accuracy of the contaminant level is questionable because of the spherical nature of the particles analyzed. The electron beam tends to scatter at different angles and may

Table 3 Summary of results from four darts launched in FSM-4

Dart no.	Elapsed time	Particles analyzed	d_{43}, contaminated	d_{43}, clean
1	12.3	3700	13.74	11.2
2	67.0	0[a]	—	—
3	68.3	4040	11.58	10.97
4	93.5	0	—	—

[a]Excessive dirt and dust mixed in with the sample because of sleeve malfunction.
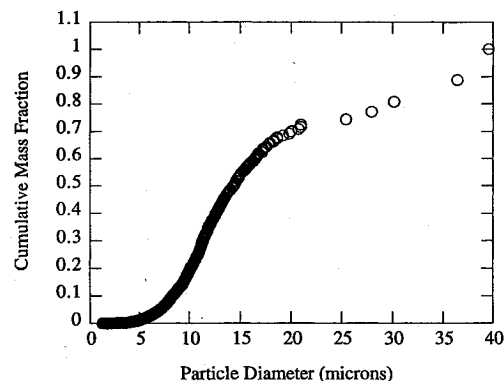
Fig. 10 Cumulative mass fraction of plume particles measured from dart 1 of FSM-4.
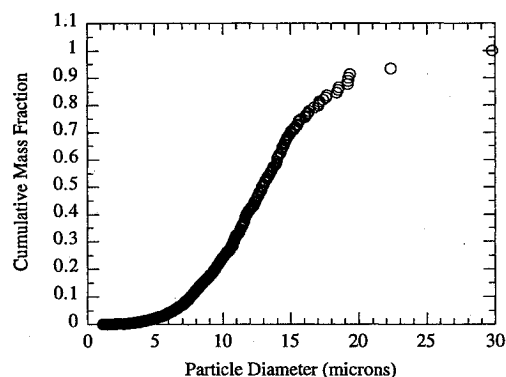
Fig. 11 Cumulative mass fraction of plume particles measured from dart 3 of FSM-4.

not be fully captured by the sensor elements in the microprobe. Similar contaminant measurements have been made by AEDC on the plume particles collected from IUS-2, PAM D-II motors[14] using spark spectroscopy. These analyses indicated contamination levels in the 1–3% range, higher than what were measured in the MNASA plume particles.

Spark spectroscopy is a more accurate method for determining the contaminant levels in the plume particles. However, a 50-mg sample would be required to perform such analysis, and the collection method employed here was not adequate to collect such large samples.

FSM-4 RSRM Motor

The results from the four darts in the FSM-4 test are summarized in Table 3. The particles collected by dart 4 appeared similar to those collected by darts 1 and 3, and consequently, a distribution was not measured from the dart 4 samples. As expected, the copper tapes from the control dart were contaminated more with ground dirt than those from the tethered darts. However, the samples were still relatively clean for discrimination of the spherical plume particles from the rough-edged dirt particles.

In FSM-4 sample analysis, dimensions of particles over 3 μm were obtained from SEM micrographs of sample areas
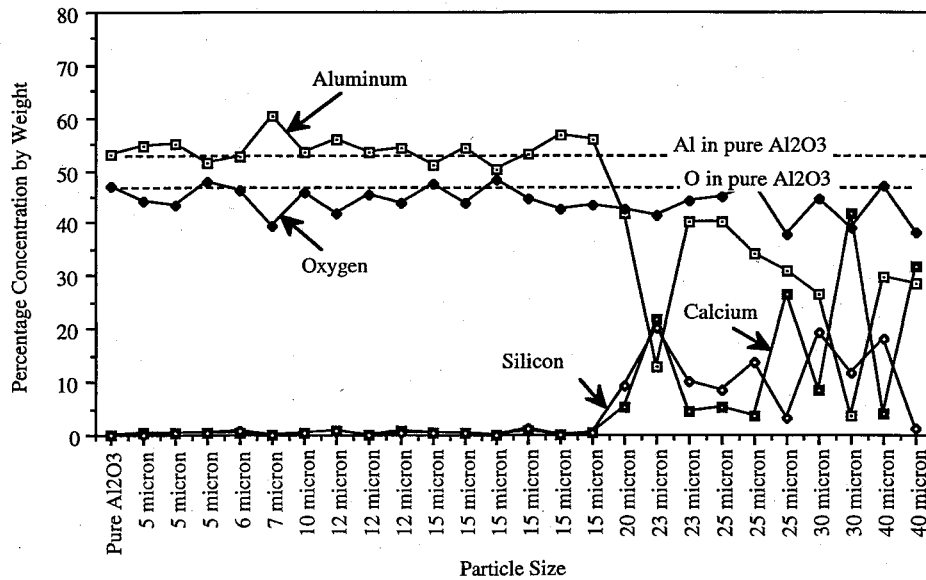
Fig. 12 Composition of discrete plume particles from FSM-4 determined from wavelength dispersive spectrums using an electron microprobe.

magnified at 250x. Dimensions of particles under 3 μm were obtained from smaller areas within the same sample area magnified at 500x. To determine the particle size distribution, the number of particles from the 500x magnifications were multiplied by 4 and added to the number of particles from the 250x magnification. Since the Al_2O_3 plume particles are expected to be spherical because of the surface tension forces in the liquid-phase droplets during their traverse through the nozzle, any nonspherical particles collected on the tape were not included in the size distribution analysis. Spherical particles stuck together were included and each particle in the cluster was measured individually. The Hermsen correlation d_{43} for the FSM-4 conditions was calculated to be 11.68 μm, and is primarily dictated by the throat diameter.

Figure 10 shows the cumulative mass plotted against the particle diameter for the plume particle sample collected by the tethered dart launched at 12.3 s after motor ignition. A total of 3700 particles was measured to obtain this distribution. These spherical particles were obtained from two SEM micrographs of random locations on two different tapes from the same dart. Only five particles among these 3700 were above 23 μm. For this sample, the test-derived d_{43} was determined to be 13.74 μm.

Figure 11 shows the cumulative mass plotted against the particle diameter for the plume sample collected by the control dart launched at 68.3 s after motor ignition. The chamber pressure of the motor is about 630 psi at this time frame. A total of 4040 particles was measured to obtain this distribution and these particles were obtained in the same manner as described previously. Only two particles among these 4040 were above 23 μm. The test-derived d_{43} was determined to be 11.58 μm.

As described before, the composition of the plume particles was determined from the wavelength dispersive spectrum of the individual particles using an electron microprobe. These plume particles were chosen randomly from samples from the two darts. A total of 26 particles was analyzed varying in diameter from 5 to 40 μm. The results of the analysis are illustrated in Fig. 12. The results clearly indicate that the plume particles in the 23–40 μm range were heavily contaminated with calcium and silicon from the ground. These contaminants were not restricted to the surface of the particles. Therefore, these large particles were assumed to be a result of the plume/ground interaction and were removed from the data set. Particles below this size range were primarily aluminum-oxide particles.
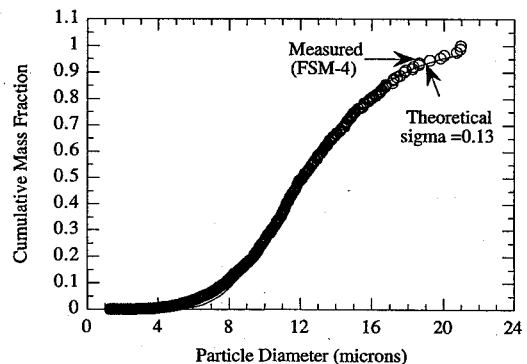

Fig. 13 Cumulative mass fraction of measured plume particles below 23 μm from dart 1. Best fit of the measured data is given by a log-normal curve with a standard deviation of 0.13.
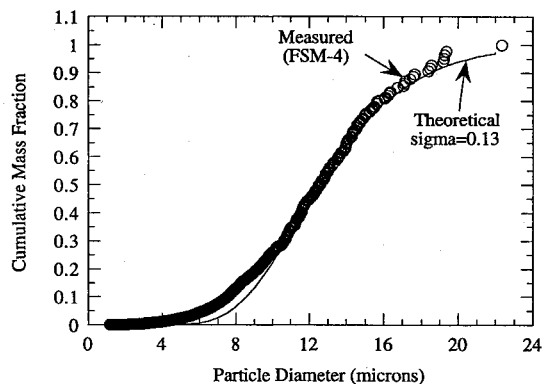

Fig. 14 Cumulative mass fraction of measured plume particles below 23 μm from dart 3. Best fit of the measured data is given by a log-normal curve with a standard deviation of 0.13.

Figure 13 shows a reformulation of the cumulative mass distribution for the plume particle sample collected by the tethered dart launched at 12.3 s after motor ignition. In this plot, all particles 23 μm and above were deleted because of the results of the electron microprobe analysis. The test-derived d_{43} is reduced from 13.74 to 11.2 μm. Also shown in this figure is the best fit of the data; a monomodal log-normal distribution with a standard deviation of 0.13. Figure 14 shows a

similar plot for the sample collected by the control dart launched at 68.3 s. The mass-averaged diameter is reduced to 10.97 μm and the best-curve-fit is again described by a monomodal log-normal distribution with a standard deviation of 0.13. These distributions agree extremely well with that predicted by Salita[10] at the exit plane of the full-scale RSRM using the OD3P code. In addition, the standard deviation measured in RSRM is almost identical to that measured in MNASA 9.

The mass-averaged diameter measured from the FSM-4 plume particle samples was smaller compared to the 11.68 μm calculated using Hermsen's correlation and the 13.2 μm (after correction to room temperature) predicted by Salita[10] at the nozzle exit plane. This could be because of the fact that these samples were collected 300 ft aft of the nozzle exit plane where the few largest particles might have already precipitated out. Another possible reason could be the omission of particles above 23 μm, since these omitted particles could have contributed to the mass fraction of the larger particles if they were not contaminated. However, the measured mass-averaged diameter of the FSM-4 plume particle samples is well within the standard deviation of the Hermsen's model, $\sigma = 0.298$ (corresponding to a deviation in d_{43} of about $\pm 35\%$).

Conclusions

It has been demonstrated that the dart system developed for the MNASA program can be adapted for collecting Al_2O_3 plume particle samples from static firings of the full-scale RSRM motor. This is the first time that plume particle samples have been obtained during the static firing of the RSRM motor. The d_{43} measured from these samples agrees with that calculated using the industry standard Hermsen's correlation within the standard deviation of the correlation. The measured cumulative mass fraction of the aluminum-oxide plume particles, plotted as a function of the particle diameter measured from each of the samples analyzed from both MNASA and RSRM motors, agreed well with the distribution theoretically predicted by Salita at the exit plane of the RSRM nozzle, and was best represented by a monomodal log-normal distribution with a standard deviation between 0.13–0.17. This agreement seems to confirm the scenario that Al_2O_3 droplet collision/coalescence in the nozzle substantially reduces the smoke mass in the plume, but still allows a comparable number density of smoke and coarse particles in the plume, which might explain the biases of the experimental procedures used in the community.

Acknowledgments

References

[1]Reardon, J. E., "Rocket Plume Base Heat Transfer Methodology," AIAA Paper 93-2823, July 1993.

[2]Nelson, H. F., "Backward Monte Carlo Modeling for Rocket Plume Base Heating," *Journal of Thermophysics and Heat Transfer*, Vol. 6, No. 3, 1992, pp. 556–558.

[3]Smith, S. D., "High Altitude Chemically Reacting Gas Particle Mixtures Volume III—Computer Code User's and Application Manual," Lockheed Missiles and Space Co.–Huntsville Research Engineering Center, TR D867400, Oct. 1984.

[4]Salita, M., "Survey of Recent Al_2O_3 Droplet Size Data in Solid Rocket Chambers, Nozzles, and Plumes," Chemical Propulsion Information Agency Publication 620, Vol. 1, Oct. 1994, pp. 1–17.

[5]Hermsen, R. W., "Aluminum Oxide Particle Size for Solid Rocket Motor Performance Prediction," *Journal of Spacecraft and Rockets*, Vol. 18, No. 6, 1981, pp. 483–490.

[6]Kohlbeck, J. A., Elmslie, J. S., Wolf, S. D., and Mitchell, E. M., "Al_2O_3 Collection from Exhaust Plumes of Full-Scale Motor Tests," *25th JANNAF Meeting*, Vol. III, Chemical Propulsion Information Agency Publication 498, Oct. 1988, pp. 293–297.

[7]Dill, K. M., Reed, R. A., Calia, V. S., and Schulz, R. Z., "Analysis of Crystalline Phase Aluminum Oxide Particles from Solid Propellant Exhausts," *Journal of Propulsion and Power*, Vol. 6, No. 5, 1990, pp. 668–671.

[8]Strand, L. D., Bowyer, J. M., Varsi, G., Laue, E. G., and Gauldin, R., "Characterization of the Exhaust Particulates in the Ground Cloud and High Altitude Plume of Large Solid Propellant Booster Rockets," *Journal of Spacecraft and Rockets*, Vol. 18, No. 4, 1981, pp. 297–305.

[9]Cofer, W. R., Lala, G. G., and Wightman, J. P., "Analysis of Mid-Tropospheric Space Shuttle Exhausted Aluminum Oxide Particles," *Atmospheric Environment*, Vol. 21, No. 5, 1987, pp. 1187–1196.

[10]Salita, M., "Implementation and Validation of the One Dimensional Gas/Particle Flow Code OD3P," *25th JANNAF Combustion Meeting*, Chemical Propulsion Information Agency Publication 498, Oct. 1988, pp. 69–82.

[11]Laredo, D., McCrorie, J. D., Vaughn, J. K., and Netzer, D. W., "Motor and Plume Particle Size Measurements in Solid Propellant Micromotors," *Journal of Propulsion and Power*, Vol. 10, No. 3, 1994, pp. 410–418.

[12]Gomes, P. V., Roddenberry, D. S., Snaza, C. J., Yakin, B., Yi, C. M., and Netzer, D. W., "Nozzle Geometry and Additive Effects on Plume Particulate Behavior in Subscale Solid Propellant Rocket Motors," *21st JANNAF Exhaust Plume Technology Subcommittee Meeting*, Vol. II, Chemical Propulsion Information Agency Publication 621, Oct. 1994, pp. 25–36.

[13]Konopka, W. L., Reed, R. A., and Calia, V. S., *Measurements of Infrared Optical Properties of Al_2O_3 Rocket Particles*, Vol. 91, Progress in Astronautics and Aeronautics, AIAA, New York, 1984.

[14]Calia, V. S., Celentano, A., Soel, M., Konopka, W., Gutowski, R., and Ryan, R., "Measurements of UV/VIS/LWIR Optical Properties of Al_2O_3 Particles," *18th JANNAF Exhaust Plume Technology Subcommittee Meeting*, Chemical Propulsion Information Agency Publication 530, Nov. 1989, pp. 183–192.